Medicinska istaživanja 2024; 57(2):75-83 | DOI 10.5937/medi57-48847

OPEN ACCESS

Medical Research | Published by Faculty of Medicine University of Belgrade

ORIGINAL ARTICLE

Multifractal characterization of grayscale histopathological images: unveiling patterns linked to metastases in breast cancer

Zorana Nedeljković[1], Dejana Milošević[2], Marko Radulović[3], Nebojša Milošević[1], Nemanja Rajković[1]

[1] University of Belgrade, Faculty of Medicine, Department of Biophysics in Medicine, Belgrade, Serbia

[2] University of Belgrade, Faculty of Medicine, Belgrade, Serbia

[3] Institute for Oncology and Radiology, Department of Experimental Oncology, Belgrade, Serbia

Recived: 22 January 2024

Revised: 26 March 2024

Accepted: 10 April 2024

Check for updates

Funding information:
This work was supported by the Serbian Ministry of Education, Science and Technological Development, grant number 451-03-66/2024-03/200110

Competing interests:
The authors have declared that no competing interests exist

Correspondence to:
Nemanja Rajković

University of Belgrade, Faculty of Medicine, Department of Biophysics in Medicine, 26/2, Visegradska Street, 11000, Belgrade, Serbia

E-mail: nemanja.rajkovic@med.bg.ac.rs

Summary

Introduction: Breast cancer, a pervasive global malignancy, demands precise prognostication of the risk of metastases for personalized therapeutic strategies and enhanced survival rates. In pursuit of refined diagnostic methodologies, this study employs multifractal analysis on grayscale histopathological images, revealing distinctive patterns associated with the occurrence of metastases.

Aim: Analyzing the multifractal spectra of grayscale images for groups with and without metastases to assess the utility of this analytical approach in enhancing the diagnostic process.

Materials and methods: The study included 102 female patients treated at the Institute for Oncology and Radiology of Serbia in the same year (1993). Histopathological samples were immunostained with a pan-cytokeratin antibody and digitized with a high-resolution scanner, from which a specialist chose representative parts, thus leading to a total number of 519 images (418 in no-metastases group and 101 in metastases group). Images were subjected to multifractal analysis, assessing the generalized dimension, Hölder exponent, and singularity spectra.

Results: Statistical comparisons between groups with and without metastases unveil significant differences in the negative domains of both generalized dimension and Hölder exponent spectra, highlighting the influence of fine structures in tissue morphology that are linked to metastatic risk.

Conclusion: Multifractal analysis applied to images of histopathological samples from breast tumors demonstrates the ability to differentiate between groups of patients with and without metastases. While caution is warranted regarding image resolution limitations and immunostaining sensitivity, this method is a non-training-dependent approach with potential diagnostic significance and possible synergies with advanced neural network approaches.

Key words: multifractal, histopathology, breast cancer, metastasis

Cite this article as: Nedeljković Z, Milošević D, Radulović M, Milošević N, Rajković N. Multifractal characterization of grayscale histopathological images: unveiling patterns linked to metastases in breast cancer Medicinska istaživanja 2024; 57(2):75-83 DOI: 10.5937/medi57-48847

INTRODUCTION

Breast cancer is the most commonly diagnosed form of malignancy in the world and is the primary cause of cancer-related death in women (1,2). Metastases pose a significant challenge in breast cancer treatment, with the occurrence of distant metastases displaying exceptional variability. Accurately prognosticating the risk of metastases becomes pivotal for tailoring individual therapeutic regimens and improving survival rates. Precision medicine holds the potential to optimize treatment strategies, with less intense interventions for low-risk individuals and intensified therapies for those reliably identified as high-risk for metastases. Currently, the reliance on cytotoxic therapy to eliminate distant micro metastases, while effective for some, subjects many breast cancer patients to unnecessary toxic side effects (3,4). By refining prognostication, the field of oncology can move towards individualized treatment plans that enhance patient survival rates while mitigating the adverse effects of chemotherapy.

Non-invasive techniques, such as mammography and breast ultrasound, serve as valuable tools for tumor detection; however, histopathological images remain the gold standard in breast cancer diagnosis (5,6). The morphological information conveyed by histopathological images offers essential prognostic insights into the molecular biology of breast cancer (7). Nevertheless, visual assessment of tumor morphology by specialists presents challenges manifested in frequent non-reproducibility of results, thereby compromising the reliability of prognostic information (8). To address this, computer image analysis emerges as a potential solution, potentially offering enhanced reliability and reduced susceptibility to error in the diagnostic process. In recent years, various approaches within the realm of computer image analysis have been proposed to address these challenges in breast cancer diagnosis (9–12), among them multifractal analysis, which exhibits promise in distinction between abnormal and healthy tissue (13,14).

Multifractal analysis sprung from fractal geometry formulated by Benoit Mandelbrot with the aim of describing the complexity of living forms in nature (15). While histopathological images qualify as natural forms, they diverge from mathematically abstract fractal patterns by manifesting fractal properties solely at limited scales (16,17). Nonetheless, the morphology of natural patterns can be effectively quantified through the application of fractal and multifractal formalism. In contrast to monofractal analysis, multifractal approaches prove more adept at describing the irregularities inherent in natural objects. Given that natural entities typically lack universal or statistical self-similarity and exhibit an uneven distribution of complexity, multifractal analysis accommodates variations in fractal dimensions across different points within the object (18,19). The aim of this study is to analyze the multifractal spectra of grayscale images for groups with and without metastases to assess the utility of this analytical approach in enhancing the diagnostic process.

MATERIALS AND METHODS

In this study, we used the same sample from two previous studies (3,20), where a different approach to image analysis was applied. Patient group and image acquisition information were presented there in more detail.

The study was approved by the Ethics Committee of the Institute for Oncology and Radiology (#2794-01; 14. July 2016) and conformed with The Code of Ethics of the World Medical Association (Declaration of Helsinki) printed in the British Medical Journal (July 18, 1964) and its 7th revision in 2013.

Patient group

The patient group consisted of 102 female patients treated at the Institute for Oncology and Radiology of Serbia in the same year (1993). The data were obtained without identifiers that would allow the identification of an individual patient. The median age at diagnosis was 57 years (with a range of 37–80 years). The follow-up time of patients without metastases ranged from 77 to 165 months with a median of 147 months. Time to metastases ranged between 16 and 155 months with a median of 61 months. Out of 102 patients, metastases were observed in 20 cases.

Image acquisition

The tissue was obtained during surgical removal of the tumor. From the histopathological samples of 102 patients, the pathologist selected one sample per patient that best represented the tumor. The samples were immunostained with a pan-cytokeratin antibody for the purpose of labeling groups of epithelial cells, and subsequently were digitized with a *Hamamatsu NanoZoomer-XRC12000 high-resolution digital slide scanner*. The procedure was described in more detail in previous studies (3,20). In this way, high-resolution color images were obtained from which the pathologist selected representative parts of the same size (about five per patient) to represent the original images used in the analysis. **Figure 1a** shows an example of such an image. In this way, a total of 519 digital images were extracted, 418 in no-metastases group (group 0) and 101 in metastases group (group 1). All the images had the same resolution of 1278 x 753 pixels, to avoid the systematic error caused by the fractal calculations' dependence on image resolution (21).

Color images were then converted to 8-bit grayscale images using the image processing and analysis software *ImageJ* version 1.48v, using the command *"Image - Type - 8bit"* (22) **(Figure 1b)**. Multifractal analysis described in the following text was then applied to the images to obtain the multifractal spectra of each individual image.

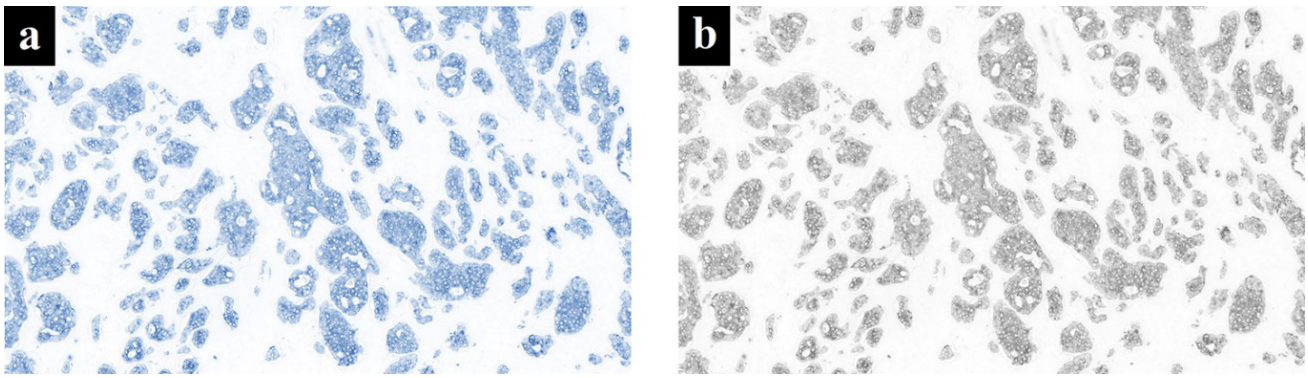

Figure 1. Representative image used in the study: a) Original color image, b) Grayscale image

Multifractal analysis

Multifractal analysis aims to quantify the morphological characteristics of an object that exhibits multiple scaling rules (23). A multifractal structure can be seen as a superposition of several homogeneous monofractal structures in a single object (24). Given the morphological nature of histopathological images, multifractal analysis can describe the statistical properties of such images that possess irregular spatial arrangements. In order to describe this "multifractality" of the objects, as well as to check whether the object is actually multifractal, we resort to the formation of a multifractal spectrum. For this purpose, an *ImageJ* plug-in called *FracLac* was used (25) whose calculations relied on the previous work of Chhabra and Jensen (26,27). We used two most commonly used spectrums – the spectrum of generalized dimensions D_Q vs Q, and singularity spectrum $f(\alpha)$ vs α, described in the following text. In addition, α vs Q and $f(\alpha)$ vs Q spectra are also represented in the study.

Analysis was implemented using the non-overlapping box count method. Spectrum of generalized dimensions D_Q vs Q is formed by using the so-called moments of order Q, which serve as a kind of distortion that mathematically emphasize different aspects of the morphology of the object (25,28). These moments are calculated for the measure $P_{(i,\varepsilon)}$ as

$$I_{[Q,\varepsilon]} = \sum_{i=1}^{N} \left[P_{(i,\varepsilon)}\right]^{Q} \quad (1)$$

where N is the total number of filled squares used in the box counting method, ε is the size of the box at the given scale, while $P_{(i,\varepsilon)}$ is the probability of a certain mass of pixels occurring in i-th box compared to the total mass at that box size ε. Hence, the generalized dimension of $D_Q(Q)$ is equal to

$$D_Q = -\lim_{\varepsilon \to 0} \frac{1}{1-Q} \frac{\ln I_{[Q,\varepsilon]}}{\ln \varepsilon} \quad (2)$$

This study is conducted on grayscale images, so the calculation of the mentioned moments is reduced to differences in pixel intensities described by the differential box counting method (25). This method calculates the difference in pixel intensities $\delta_{Ii,j,\varepsilon}$ in each square of a certain size, so it is

$$\delta_{Ii,j,\varepsilon} = max\ pixel\ intensity(i,j,\varepsilon) - min\ pixel\ intensity(i,j,\varepsilon) \quad (3)$$

This actual intensity range is increased by 1, to avoid a zero value in later calculations of the logarithm from which we have

$$I_\varepsilon = \sum \left[1 + \delta_{Ii,j,\varepsilon}\right] \quad (4)$$

Singularity spectrum $f(\alpha)$ vs α is another common type of multifractal spectrum. Parameter α is called Hölder exponent, also known as *singularity strength* (29), and it represents the degree of concentration of mass measure probability (30). Greater values of α indicate a smaller degree of concentration, and vice versa (29,30). In practice, following the calculations given by Chhabra and Jensen, we found the measure of mass probability for each box of the size ε (26,27,30)

$$\mu_{i(Q,\varepsilon)} = \frac{{P_{i(Q,\varepsilon)}}^{Q}}{\sum_{i=1}^{N} {P_{i(Q,\varepsilon)}}^{Q}} \quad (5)$$

which enabled us to calculate the coarse Hölder exponent (26,27,29,30)

$$\alpha(Q) = \frac{\sum_{i=1}^{N(\varepsilon)} \mu_{i(Q,\varepsilon)} \cdot \ln P_{i(Q,\varepsilon)}}{\ln \varepsilon} \quad (6)$$

and finally

$$f(\alpha(Q)) = \frac{\sum_{i=1}^{N(\varepsilon)} \mu_{i(Q,\varepsilon)} \cdot \ln \mu_{i(Q,\varepsilon)}}{\ln \varepsilon} \quad (7)$$

Parameter $f(\alpha)$ can be interpreted as a fractal dimension of a set of points with a singularity strength of α (30).

Values for parameter Q ranged from -10 to 10, with a step of 0.25, resulting in 81 points in the spectra of each image. Each of the 81 points in 3 different spectra (D_Q vs Q, α vs Q and $f(\alpha)$ vs Q) was treated as a separate variable for differentiation between the groups. The additional $f(\alpha)$ vs α spectrum was also presented for easier visual multifractal data comprehension, as it is the most commonly used multifractal spectrum.

Box counting algorithm was implemented with 12 different grid positions for each box size. Among the 12 positions, the one with the minimal number of boxes was chosen, reducing the possibility of error in calculations of the parameters (25). Theoretically, to avoid errors of this type altogether, the number of grid positions should be the maximum possible, depending on the image size. The number of positions in this study was chosen as a compromise between the computation time and further reducing the possibility of error, which is already quite low at 12 positions, rendering the increase unnecessary.

From the multifractal spectra $f(\alpha)$ vs α, additional parameters were extracted in order to further characterize the spectrum. Parameters included α_{min}, α_{max}, $\Delta\alpha$, $f(\alpha)_{min}$, $f(\alpha)_{max}$, $\Delta f(\alpha)$, where $\Delta\alpha$ and $\Delta f(\alpha)$ were calculated as $\alpha_{max} - \alpha_{min}$ and $f(\alpha)_{max} - f(\alpha)_{min}$, respectively.

Statistical analysis

Data analysis was performed using *IBM SPSS Statistics v25* software. The quantitative measure of the difference between the prognostic groups was evaluated by the non-parametric Mann-Whitney U test since normal distribution could not be guaranteed for all used variables. Results with p values ≤ 0.05 were considered statistically significant.

RESULTS

Considering the large number of variables in multifractal spectra, the data in this paper will be mainly presented graphically.

Spectrum of generalized dimensions $D_Q(Q)$

Figure 2 shows the median values of generalized dimension D_Q depending on the parameter Q, for both groups of patients. It is observed that with an increase in parameter Q, the values of the generalized dimension decrease, which is expected due to the sigmoid shape of this type of multifractal spectrum (25,30). The greatest drop in D_Q values is between Q = -1.5 and Q = -1.25 for group 0, and between Q = -0.75 and Q = -0.5 for group 1. Differences in median values between groups tend to decrease with increasing Q values and are greatest in the Q value range from -4.75 to -3. Statistically significant differences between groups were observed on practically entire spectrum with negative values of Q, (except for point Q = 0.25), with higher median D_Q values for group 1. The median values of the D_Q parameter are higher for group 1 on most of the spectrum except for the Q values in the range from 0.25 to 6.75, but it is worth noting that differences on the Q-positive part of the spectrum were negligible (differences were observed only in the third decimal place).

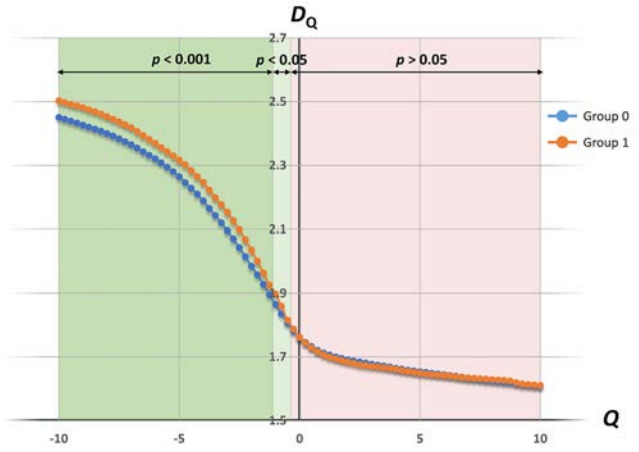

Figure 2. Spectra of median values of generalized dimensions $D_Q(Q)$. Significant differences were observed for Q values in the range of -10 to -1.25 ($p < 0.001$) and -1 to -0.5 ($p < 0.05$), indicated with green shades.

Spectrum of Hölder exponents α(*Q*)

The median value Hölder exponent spectrum $a(Q)$ is presented in **Figure 3** for both groups. This graph also exhibits a sigmoidal shape, where the median values of the Hölder exponent a decrease with increasing Q value. Statistically significant differences between the groups are found on the whole Q-negative part of the spectrum, including the Q = 0 point. On this part of the spectrum the median a values were higher for group 1, with the maximum difference in the Q range of -4 to -1. On the Q-positive part of the spectrum, similarly to $D_Q(Q)$ spectrum, the differences between the median values of a were negligible.

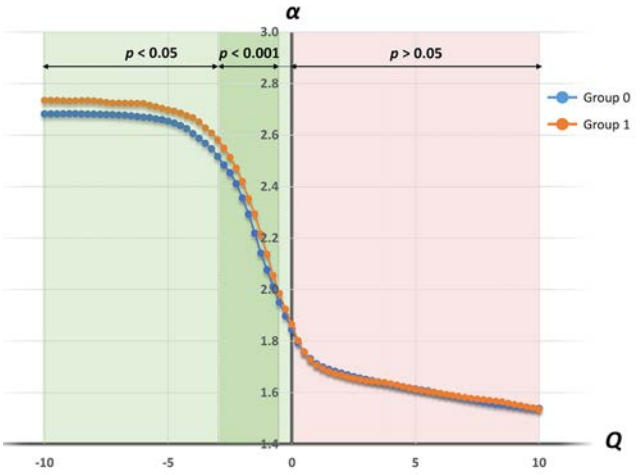

Figure 3. Spectra of median values of Hölder exponents $a(Q)$. Significant differences ($p < 0.05$) were observed for Q values in the range of -10 to 0, including the segment with $p < 0.001$ in the range of -2.75 to -0.5, indicated with green shades.

Singularity spectrum $f(\alpha)$

The graph $f(\alpha)$ vs Q is shown in **Figure 4** for both groups. Median values of $f(\alpha)$ were similar for both groups, except for three narrow parts of the spectrum: the extreme negative part ($Q < 9.5$), the middle part ($-2.25 < Q < -1.25$) and the extreme positive part ($Q = 10$), where statistically significant differences were observed. At the extreme negative part, the values of the parameter $f(\alpha)$ were higher for group 1, while on the other two segments the values were lower for the same group. This shows that both groups exhibited similar probability distribution of singularity strengths on most Q values.

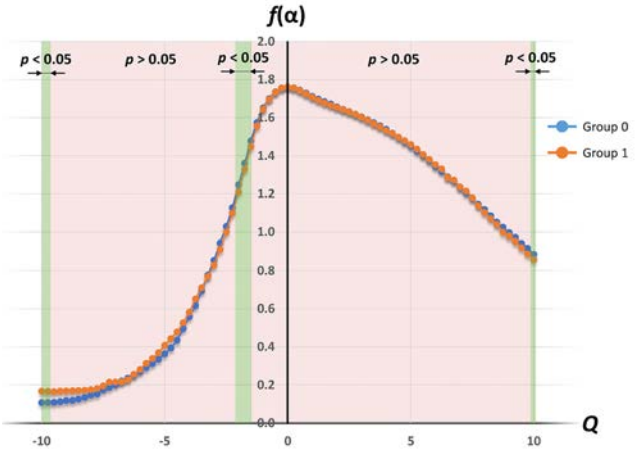

Figure 4. Spectra of median values $f(\alpha)$ vs Q. Significant differences ($p < 0.05$) were observed in narrow segments of Q values in the ranges of -10 to -9.75, -2 to -1.5 and on a single point $Q = 10$, indicated with green color.

Singularity spectra $f(\alpha)$ vs α, for both groups, are presented in **Figure 5**. Differences between the groups are observed in the right part of the spectrum, for median α values in the range of 1.844 (0.316) to 2.724 (0.792) where group 1 exhibited higher values of parameter $f(\alpha)$. This difference is mostly due to the differences in the singularity strengths α (as shown in **Figure 3**) as opposed to the differences in $f(\alpha)$ which were shown to be small **(Figure 4)**.

Table 1 contains median values and range for extreme value parameters in the $f(\alpha)$ vs α spectrum of each patient, for both groups. Parameters α_{max} and $\Delta\alpha$ showed statistically significant differences between the groups. This is consistent with the data in **Figure 3**, where we observed significant differences in the entire Q-negative part of the spectrum where the parameter α showed higher median values, including its maximum. On the other hand, minimal values of α parameter showed no significant difference between the groups. This value is contained in the Q-positive part of the spectrum where differences between the medians were very slight. None of the $f(\alpha)$ extreme value parameters (min, max and Δ) showed statistically significant differences, which is consistent with the data in **Figure 4**, where we observed differences on very narrow segments of the spectra, none of which contained these extreme values.

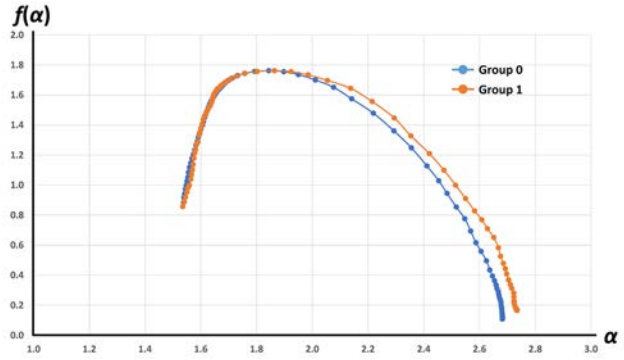

Figure 5. Singularity spectra of median values $f(\alpha)$ vs α for both groups.

Table 1. Extreme value parameters from the singularity spectra $f(\alpha)$ vs α of each patient

parameter	median value (range)		Mann-Whitney U	Z	P
	group 0	group 1			
α_{min}	1.538 (0.406)	1.535 (0.443)	20066.5	-0.771	0.441
α_{max}	2.687 (1.097)	2.736 (0.777)	25561.5	3.292	**0.001**
$\Delta\alpha$	1.153 (1.196)	1.213 (0.828)	25813.5	3.478	**0.001**
$f(\alpha)_{min}$	0.093 (1.403)	0.144 (1.296)	23553.5	1.807	0.071
$f(\alpha)_{max}$	1.762 (0.151)	1.762 (0.143)	22329.5	0.934	0.350
$\Delta f(\alpha)$	1.680 (1.489)	1.629 (1.253)	18839	-1.678	0.093

DISCUSSION

Multifractal analysis has proven to be a useful tool in quantifying the morphology of highly irregular two-dimensional objects. Images of histopathological tissue samples, including breast cancer samples, can also be included in such patterns, in a certain range of scales (13,23,28). By generating multifractal spectra, the properties of various aspects of the given object can be observed. The spectra are generated using moments of order Q, i.e., of numbers that serve as exponents that more or less emphasize the probability of the pixel distribution (Equations 1 and 5). In this way, a kind of distortion of the object is carried out, the aim of which is to accentuate different features of the object bringing them to the foreground. Thus, in the part of the spectrum with positive values of the exponent Q, the parts of the multifractal object that are more noticeable on the pattern and which contain a larger number of pixels, will prevail, while in the negative part of the spectrum, the "finer" features of the pattern that are not in the foreground will dominate (24,25). In case of the generalized dimension spectrum, the point in the central part of the spectrum (for the value $Q = 0$) is actually the Hausdorff-Besicovitch dimension, i.e., box count fractal dimension, and

describes the spatial complexity of the original object without the applied mathematical distortion (15,25). The multifractality of the object is reflected in the sigmoidal nature of its generalized dimension spectrum. The more pronounced the sigmoid shape the more heterogeneous the object in terms of the scaling rules. For example, the monofractal pattern would have a spectrum that is close to the straight line (25). We can also assess the multifractality of the object by observing the singularity spectrum ($f(\alpha)$ vs α), which exhibits a parabolic shape. The width of the spectrum (which is dictated by the range of values of the Hölder exponent α) is related to the scaling rules of heterogeneity, where wider spectra belong to the patterns with more scaling rules (i.e., multifractals) (25,30,31).

Two-dimensional histopathological images of breast tumors show multifractal characteristics (13,23,28). This multifractality can be considered a consequence of the fact that the given images contain sets of cells of various irregular shapes, so by observing an image as a whole, we include multiple scaling laws.

In the results presented in this paper, it can be noted that almost the entire part of the D_Q spectrum with negative Q moments showed statistically significant differences between the groups **(Figure 2)**. This indicates the possibility that parts of the image with a smaller number of pixels, and thus finer structures in the tissue, carry important prognostic information. The roughness of the pattern on the less pronounced parts of the image proved to be a separating factor for the two groups. This roughness is reflected in the values of the generalized fractal dimensions of D_Q, so it should be noted that the values of these parameters were slightly higher for the group with the appearance of metastases on the entire negative part of the spectrum. As all pixels of the pattern in the image represent immuno-staining with a pan-cytokeratin antibody, it can be assumed that precisely the fine morphological features of these structures in the epithelial cells contain essential information about the tumor itself. Our findings indicate that the rougher morphology of immunostained structures carries with it the higher prognostic risk.

Spectrum of Hölder exponents $\alpha(Q)$ **(Figure 3)** confirms the findings from the $D_Q(Q)$ spectrum, testifying to the dominance of fine details in the images. Regions with higher α value, i.e., the more homogenous regions in terms of local pixel intensity, showed significant differences between the groups on the entire Q-negative part of the spectrum. Observing the two spectra, $\alpha(Q)$ and $D_Q(Q)$ together, we conclude that small differences in the roughness of the finer regions of the patterns hold the key differences in terms of prognostic significance.

The biggest differences for the parameters D_Q and α were found on the parts of the spectra with Q values from around -4 to -1, which is located on the greatest slope of the sigmoidal spectra. Therefore, when trying to reduce the number of variables in this type of analysis, the mentioned region of the spectra could be of importance, as well as the variable α_{max}, which also showed statistically significant differences.

A multifractal object can be viewed as a superposition of several monofractal objects determined by a Hölder exponent α. Observed from this perspective, the function $f(\alpha)$ is actually the Hausdorff dimension of such a set of points with a monofractal structure and unique scaling law (24,30,32). The $f(\alpha)$ vs Q spectra were very similar for both groups, with only minor statistical differences **(Figure 4)**. From this we can conclude that groups had very similar probability distributions of Hölder's exponents α, i.e., they had similar distributions of scaling laws. On the other hand, the singularity spectra (presented in **Figure 5**) exhibit differences in width, with group 1 having a slightly wider spectrum. This difference $\Delta\alpha$ is statistically significant **(Table 1)**, and points to the slightly higher "multifractality" of the group 1 images. Thus, even though the overall distribution of complexity is rather similar between the groups, group 1 exhibited slightly more scaling rules. With all this taken into account, the group differences could be considered a consequence of the different degrees of complexity of individual regions, rather than fundamentally different distribution of the complexity of the overall images.

While the interpretation of our findings suggests that the fine structures within the pattern hold paramount morphological significance for diagnostic purposes, caution is warranted. The resolution of the images employed in this investigation, though relatively high (1278 x 753 pixels), introduces a potential limitation when confronted with larger distortions, as finer details are contingent upon the pixel density. Additionally, the preeminence of the immunostaining signal underscores its pivotal role in the analysis. Therefore, meticulous consideration must be given to the quality of staining, given its heightened sensitivity within the procedural framework. It is imperative to acknowledge that practical constraints limit our ability to regulate all contributing factors influencing the staining process.

It is noteworthy that, in terms of prognostic accuracy, the efficacy of the presented analysis method falls somewhat short when juxtaposed with convolutional neural networks (18,28,33–35). Conversely, neural networks exhibit drawbacks such as a requisite for substantial training datasets, high computational demands, and a narrow applicability confined to images closely resembling those encountered during training (36–38). In contrast, fractal and textural analysis methods possess the advantage of independence from training requirements, potentially offering a means to quantify investigated morphology and support specialists in decision-making (13,18,33,39). Subsequent investigations may explore synergies between these methodologies, integrating fractal and textural features as inputs into neural networks (40).

Examining the tissue holistically presents an additional advantage inherent to these analyses. This approach mitigates systematic errors that may arise from

further image segmentation or the isolation of individual elements. Furthermore, it affords a comprehensive overview of the entire information embedded in the image, avoiding oversight of critical details that could occur through the selective extraction of specific objects (28).

CONCLUSION

Multifractal analysis applied to gray-scale images of histopathological samples from breast tumors demonstrates the ability to differentiate between groups of patients with and without metastases. Statistically significant distinctions emerge in the negative domains of both the generalized dimension and Hölder exponent multifractal spectra between these patient groups. With further research, this type of analysis could potentially be a useful auxiliary tool in the diagnosis and the selection of treatment strategies for this disease.

Conflict of interest

The authors declare that they do not have any conflicts of interest.

Ethical approval

The study was approved by the Ethics Committee of the Institute for Oncology and Radiology and conforms with The Code of Ethics of the World Medical Association (Declaration of Helsinki).

REFERENCES

1. Sung H, Ferlay J, Siegel RL, Laversanne M, Soerjomataram I, Jemal A, et al. Global Cancer Statistics 2020: GLOBOCAN Estimates of Incidence and Mortality Worldwide for 36 Cancers in 185 Countries. CA Cancer J Clin [Internet]. 2021;71(3):209–49. DOI: https://doi.org/10.3322/caac.21660
2. Ferlay J, Colombet M, Soerjomataram I, Parkin DM, Piñeros M, Znaor A, et al. Cancer statistics for the year 2020: An overview. Int J cancer. 2021 Apr; DOI: 10.1002/ijc.33588
3. Vranes V, Rajković N, Li X, Plataniotis KN, Raković NT, Milovanović J, et al. Size and Shape Filtering of Malignant Cell Clusters within Breast Tumors Identifies Scattered Individual Epithelial Cells as the Most Valuable Histomorphological Clue in the Prognosis of Distant Metastasis Risk. Cancers (Basel) [Internet]. 2019;11(10). DOI: 10.3390/cancers11101615
4. Shaked Y. Balancing efficacy of and host immune responses to cancer therapy: the yin and yang effects. Nat Rev Clin Oncol [Internet]. 2016;13(10):611–26. DOI: 10.1038/nrclinonc.2016.57
5. R R, Prasad K, Udupa CBK. BCHisto-Net: Breast histopathological image classification by global and local feature aggregation. Artif Intell Med [Internet]. 2021;121:102191. DOI: https://doi.org/10.1016/j.artmed.2021.102191
6. Lakhani SR, Ellis IO, Schnitt S, Tan PH, van de Vijver M. WHO Classification of Tumours of the Breast. 4th editio. IARC; 2012.
7. Hanby AM. The pathology of breast cancer and the role of the histopathology laboratory. Clin Oncol [Internet]. 2005;17(4):234–9. DOI: https://doi.org/10.1016/j.clon.2005.02.009
8. Ojansivu V, Linder N, Rahtu E, Pietikäinen M, Lundin M, Joensuu H, et al. Automated classification of breast cancer morphology in histopathological images. Diagn Pathol [Internet]. 2013;8(1):S29. DOI: 10.1186/1746-1596-8-S1-S29
9. Farahnaz Sadoughi Zahra Kazemy FHLOMR, Azadboni TT. Artificial intelligence methods for the diagnosis of breast cancer by image processing: a review. Breast Cancer Targets Ther [Internet]. 2018;10:219–30. DOI: 10.2147/BCTT.S175311
10. Robertson S, Azizpour H, Smith K, Hartman J. Digital image analysis in breast pathology—from image processing techniques to artificial intelligence. Transl Res [Internet]. 2018;194:19–35. DOI: https://doi.org/10.1016/j.trsl.2017.10.010
11. da Silva LG, da Silva Monteiro WRS, de Aguiar Moreira TM, Rabelo MAE, de Assis EACP, de Souza GT. Fractal dimension analysis as an easy computational approach to improve breast cancer histopathological diagnosis. Appl Microsc [Internet]. 2021;51(1):6. DOI: 10.1186/s42649-021-00055-w
12. Mohammed MA, Al-Khateeb B, Rashid AN, Ibrahim DA, Abd Ghani MK, Mostafa SA. Neural network and multi-fractal dimension features for breast cancer classification from ultrasound images. Comput Electr Eng [Internet]. 2018;70:871–82. DOI: https://doi.org/10.1016/j.compeleceng.2018.01.033
13. Vasiljevic J, Pribic J, Kanjer K, Jonakowski W, Sopta J, Nikolic-Vukosavljevic D, et al. Multifractal analysis of tumour microscopic images in the prediction of breast cancer chemotherapy response. Biomed Microdevices [Internet]. 2015;17(5):93. DOI: 10.1007/s10544-015-9995-0
14. Joseph AJ, Pournami PN. Multifractal theory based breast tissue characterization for early detection of breast cancer. Chaos, Solitons & Fractals [Internet]. 2021;152:111301. DOI: https://doi.org/10.1016/j.chaos.2021.111301
15. Mandelbrot BB. The Fractal Geometry of Nature [Internet]. Vol. 51, American Journal of Physics. 1983. 286 p. DOI: 10.1017/CBO9781107415324.004
16. Pribic J, Vasiljevic J, Kanjer K, Konstantinovic ZN, Milošević NT, Vukosavljevic DN, et al. Fractal dimension and lacunarity of tumor microscopic images as prognostic indicators of clinical outcome in early breast cancer. Biomark Med. 2015;9(12):1277–9. DOI: 10.2217/bmm.15.102
17. Braverman B, Tambasco M. Scale-specific multifractal medical image analysis. Comput Math Methods Med. 2013;2013. DOI: 10.1155/2013/262931
18. Rajković N, Kolarević D, Kanjer K, Milošević NT, Nikolić-Vukosavljević D, Radulovic M. Comparison of Monofractal, Multifractal and gray level Co-occurrence matrix algorithms in analysis of Breast tumor microscopic images for prognosis of distant metastasis risk. Biomed Microdevices. 2016;18(5). DOI: 10.1007/s10544-016-0103-x
19. Smith TG, Lange GD, Marks WB. Fractal methods and results in cellular morphology - Dimensions, lacunarity and multifractals. Vol. 69, Journal of Neuroscience Methods. 1996. p. 123–36. DOI: 10.1016/S0165-0270(96)00080-5
20. Vranes V, Vujasinović T, Rajković N, Kanjer K, Milošević NT, Radulovic M. Analysis of Spatial Distribution and Prognostic Value of Different Pan Cytokeratin Immunostaining Intensities in Breast Tumor Tissue Sections. Int J Mol Sci [Internet]. 2020;21(12):4434. DOI: 10.3390/ijms21124434
21. Rajković N, Krstonošić B, Milošević NT. Box-Counting Method of 2D Neuronal Image: Method Modification and Quantitative Analysis Demonstrated on Images from the Monkey and Human Brain. Comput Math Methods Med. 2017;2017(8967902):9. DOI: 10.1155/2017/8967902
22. Schneider CA, Rasband WS, Eliceiri KW. NIH Image to ImageJ: 25 years of image analysis. Nat Meth. 2012 Jul;9(7):671–5.

23. Rajković N, Stojadinović B, Radulovic M, Milošević NT. Histological Images of Malignant Breast Tumor: Mono and Multifractal Analysis. In: 2015 20th International Conference on Control Systems and Computer Science. 2015. p. 531–8. DOI: 10.1109/CSCS.2015.52
24. Lopes R, Betrouni N. Fractal and multifractal analysis: A review. Med Image Anal [Internet]. 2009;13(4):634–49. DOI: https://doi.org/10.1016/j.media.2009.05.003
25. Karperien AL. FracLac for ImageJ [Internet]. Charles Sturt University; 2013. Available at: https://imagej.net/ij/plugins/fraclac/FLHelp/Introduction.htm
26. Chhabra A, Jensen R V. Direct determination of the f(α) singularity spectrum. Phys Rev Lett [Internet]. 1989 Mar;62(12):1327–30. DOI: 10.1103/PhysRevLett.62.1327
27. Chhabra AB, Meneveau C, Jensen R V., Sreenivasan KR. Direct determination of the f(α) singularity spectrum and its application to fully developed turbulence. Phys Rev A. 1989;40(9):5284–94. DOI: 10.1103/PhysRevA.40.5284
28. Rajković N, Radulovic M, Stojadinović B, Nikolić-Vukosavljević D, Kranjer K, Milošević NT. Analysis of Histopathology Images by the Use of Monofractal and Multifractal Algorithms. In: 2017 21st International Conference on Control Systems and Computer Science (CSCS). 2017. p. 350–5. DOI: 10.1109/CSCS.2017.54
29. Evertsz CJG, Mandelbrot BB. Multifractal Measures. In: Peitgen HO, Jurgens H, Saupe D, editors. Chaos and Fractals. Springer-Verlag New York; 1992. p. 921–53.
30. San José Martínez F, Martín MA, Caniego FJ, Tuller M, Guber A, Pachepsky Y, et al. Multifractal analysis of discretized X-ray CT images for the characterization of soil macropore structures. Geoderma [Internet]. 2010;156(1):32–42. DOI: https://doi.org/10.1016/j.geoderma.2010.01.004
31. Albuquerque EL, Cottam MG. Chapter 6 - Plasmon-Polaritons in Quasiperiodic Structures. In: Albuquerque EL, Cottam MG, editors. Polaritons in Periodic and Quasiperiodic Structures [Internet]. Amsterdam: Elsevier Science; 2004. p. 125–56. DOI: https://doi.org/10.1016/B978-044451627-5/50006-7
32. Abry P, Jaffard S, Wendt H. Irregularities and scaling in signal and image processing: multifractal analysis. In: Benoit Mandelbrot [Internet]. 2015. p. 31–116. DOI: 10.1142/9789814366076_0003
33. Rajković N, Li X, Plataniotis KN, Kanjer K, Radulovic M, Milošević NT. The Pan-Cytokeratin Staining Intensity and Fractal Computational Analysis of Breast Tumor Malignant Growth Patterns Prognosticate the Occurrence of Distant Metastasis. Front Oncol [Internet]. 2018;8:348. DOI: 10.3389/fonc.2018.00348
34. Anwar SM, Majid M, Qayyum A, Awais M, Alnowami M, Khan MK. Medical Image Analysis using Convolutional Neural Networks: A Review. J Med Syst [Internet]. 2018;42(11):226. DOI: 10.1007/s10916-018-1088-1
35. Dutta P, Upadhyay P, De M, Khalkar RG. Medical Image Analysis using Deep Convolutional Neural Networks: CNN Architectures and Transfer Learning. In: 2020 International Conference on Inventive Computation Technologies (ICICT). 2020. p. 175–80. DOI: 10.1109/ICICT48043.2020.9112469
36. Yu H, Yang LT, Zhang Q, Armstrong D, Deen MJ. Convolutional neural networks for medical image analysis: State-of-the-art, comparisons, improvement and perspectives. Neurocomputing [Internet]. 2021;444:92–110. DOI: https://doi.org/10.1016/j.neucom.2020.04.157
37. Zhang C, Bengio S, Hardt M, Recht B, Vinyals O. Understanding Deep Learning (Still) Requires Rethinking Generalization. Commun ACM [Internet]. 2021 Feb;64(3):107–115. DOI: 10.1145/3446776
38. Goodfellow I, Bengio Y, Courville A. Deep Learning [Internet]. MIT Press; 2016. (Adaptive Computation and Machine Learning series).
39. Djuričić GJ, Rajković N, Milošević N, Sopta JP, Borić I, Dučić S, et al. Computational analysis of MRIs predicts osteosarcoma chemoresponsiveness. Biomark Med [Internet]. 2021;15(12):929–40. DOI: 10.2217/bmm-2020-0876
40. Pantic I, Paunovic Pantic J, Radojevic-Skondric S. Application of fractal and textural analysis in medical physiology, pathophysiology and pathology. Med Istraz. 2022;55(3):43–51. DOI: 10.5937/medi55-40351

MULTIFRAKTALNA ANALIZA NA HISTOPATOLOŠKIM SLIKAMA U SIVIM TONOVIMA: OTKRIVANJE OBRAZACA POVEZANIH SA POJAVOM METASTAZA KOD RAKA DOJKE

Zorana Nedeljković[1], Dejana Milošević[2], Marko Radulović[3], Nebojša Milošević[1], Nemanja Rajković[1]

Sažetak

Uvod: Rak dojke, sveprisutni globalni malignitet, zahteva preciznu prognozu rizika od metastaza za personalizovane terapijske strategije i povećane stope preživljavanja. U potrazi za unapređenim dijagnostičkim metodologijama, ova studija koristi multifraktalnu analizu na histopatološkim slikama u sivim tonovima, otkrivajući karakteristične obrasce povezane sa pojavom metastaza.

Cilj: Analizirati multifraktalne spektre slika histopatoloških uzoraka za grupe sa i bez metastaza kako bi se procenila korisnost ovog analitičkog pristupa u poboljšanju dijagnostičkog procesa.

Materijali i metode: Istraživanjem su obuhvaćene 102 pacijentkinje lečene iste godine (1993) na Institutu za onkologiju i radiologiju Srbije. Histopatološki uzorci su imunobojeni pancitokeratin antitelom i digitalizovani skenerom visoke rezolucije, od kojih je specijalista birao reprezentativne delove, što je dovelo do ukupnog broja od 519 slika (418 u grupi bez metastaza i 101 u grupi sa metastazama). Slike su podvrgnute multifraktalnoj analizi, procenjujući spektre generalizovanih dimenzija, Holderovih eksponenata i singulariteta.

Rezultati: Statistička poređenja između grupa sa i bez metastaza otkrivaju značajne razlike u negativnim domenima spektara generalizovanih dimenzija i Holderovih eksponenata, naglašavajući uticaj finih struktura u morfologiji tkiva koje su povezane sa rizikom od metastaza.

Zaključak: Multifraktalna analiza primenjena na slike histopatoloških uzoraka tumora dojke pokazuje sposobnost razlikovanja grupa pacijenata sa i bez metastaza. Iako je potreban oprez u pogledu ograničenja, poput uticaja rezolucije slike i osetljivosti na imunološko bojenje, ovaj metod ne zavisi od treninga na velikom uzorku i pokazuje potencijalni dijagnostički značaj kao i moguću sinergiju sa naprednim neuronskim mrežama.

Ključne reči: multifraktal, histopatologija, rak dojke, metastaze

Primljen: 22.01.2023. I **Revizija:** 26.03.2024. I **Prihvaćen:** 10.04.2024.

Medicinska istaživanja 2024; 57(2):75-83